12-9-2013

# Limit for thermal transport reduction in Si nanowires with nanoengineered corrugations

Sean E. Sullivan
*Univiversity of Texas Austin*

Keng-Hua Lin
*Purdue University*, lin105@purdue.edu

Stanislav Avdoshenko
*Purdue University*, savdoshe@purdue.edu

Alejandro Strachan
*Purdue University, Birck Nanotechnology Center*, strachan@purdue.edu

AIP | Applied Physics Letters

# Limit for thermal transport reduction in Si nanowires with nanoengineered corrugations

Sean E. Sullivan, Keng-Hua Lin, Stanislav Avdoshenko, and Alejandro Strachan

Citation: Applied Physics Letters **103**, 243107 (2013); doi: 10.1063/1.4844995
View online: http://dx.doi.org/10.1063/1.4844995
View Table of Contents: http://scitation.aip.org/content/aip/journal/apl/103/24?ver=pdfcov
Published by the AIP Publishing

# Limit for thermal transport reduction in Si nanowires with nanoengineered corrugations

Sean E. Sullivan,[a] Keng-Hua Lin, Stanislav Avdoshenko, and Alejandro Strachan[b]
*School of Materials Engineering and Birck Nanotechnology Center, Purdue University, West Lafayette, Indiana 47907, USA*

(Received 1 October 2013; accepted 22 November 2013; published online 11 December 2013)

Non-equilibrium molecular dynamics simulations reveal that the thermal conductance of Si nanowires with periodic corrugations is lower than that of smooth wires with cross-sections equivalent to the constricted portions. This reduction in conductance is up to 30% and tends to plateau with increasing corrugation height. Spatially resolved temperature and heat current maps provide a microscopic understanding of this effect; we find that 80% of the heat current is carried through the constricted area even for high-amplitude corrugations. More importantly, we show that temperature gradient inversion and heat current vortices at the ridge peaks establish fundamental limits on maximum conductance reduction. © *2013 AIP Publishing LLC*. [http://dx.doi.org/10.1063/1.4844995]

Thermal transport in complex nanostructured materials is increasingly important in areas such as nanoelectronics and energy conversion.[1,2] As we move toward smaller and more complex three-dimensional device architectures in nanoelectronics, power densities continue to increase and new solutions based on a fundamental understanding of thermal transport at the nanoscale are required. Tuning phonon and electron transport using nanoengineering is also critical in thermoelectric applications where the figure of merit, ZT, is optimized by minimizing thermal conductivity while simultaneously maximizing electronic conductivity.

Silicon nanowires (SiNWs) have been investigated for several years for their possible application in both thermoelectric energy conversion,[3] as well as next-generation transistors.[4] Additionally, the effects of surface roughness on their thermal transport have been well documented.[5–9] Roughness introduced by etching,[10] as well as surface amorphization[11] has been demonstrated to reduce thermal conductivity and conductance values by orders of magnitude, experimentally and theoretically. However, less is known about thermal transport in crystalline wires nanoengineered to have specific structural features.

Nanowires with periodically modulated cross-sections have been studied theoretically using the Boltzmann transport equation.[12,13] Both studies found a reduction in phonon thermal transport due to modulation. A sharp sawtooth surface roughness was found to induce phonon backscattering, reducing the thermal conductance below the diffusive surface limit.[12] It was also shown that modulated cross-sections in thin square nanowires reduced the phonon thermal flux by about a factor of five at $T = 300\,K$.[13] In this case, the reduction was attributed to the trapping of certain phonon modes within the modulated sections of wire, thus preventing them from contributing to heat flow. In both cases, the conductance reduction by nanoscale surface features appears to exhibit a fundamental limit, but the associated physics are not well understood.

In this Letter, we investigate the effects of nanoscale surface modulation on longitudinal thermal transport for Si nanowires, focusing on the effects of the height of corrugation. We use molecular dynamics (MD) simulations; this technique solves the many body problem on an atomic basis and makes no assumptions about scattering mechanisms, anharmonicity, and surface processes, see, for example Ref. 14. The simulations enable the characterization of local temperature and heat flux with near-atomic resolution and reveal a microscopic picture where temperature gradient inversion and heat current vortex formations are essential for understanding localized thermal transport within the corrugations. Structures with similar geometries have been studied on the macroscale. Corrugation is often used in heat pipes and other thermal conduction channels to enhance heat transfer between the cooling fluid and the dissipater.[15] These geometries also result in altered fluid flow and, at high corrugation amplitudes, turbulent flow detachment and vorticity.[16,17] Recently, silicon nanowires with engineered periodic corrugations on the order of hundreds of nanometers have been experimentally shown to exhibit unique thermal transport behavior.[18] Heat conduction below the Casimir limit at low temperatures in these structures has been attributed to a significant reduction in phonon mean free path and multiple scattering processes due to the corrugation.

We characterize thermal conduction in a family of corrugated nanowires with radius varying sinusoidally with position along the transport direction as

$$R(z) = R_0 + \Delta R \cos(2\pi z/\lambda), \quad (1)$$

where $R_0$ is the mean radius, $\Delta R$ is the corrugation amplitude, and $\lambda$ is its period. A prototypical corrugated Si nanowire (CSiNW) is shown in Fig. 1(a). We impose periodic boundary conditions along the transport direction and characterize wires with a periodic length of 40 nm along the [110] crystallographic direction. The corrugation period is one forth of the

[a]Present address: Materials Science and Engineering Program, University of Texas at Austin, Austin, Texas 78712, USA.
[b]Electronic mail: strachan@purdue.edu

 

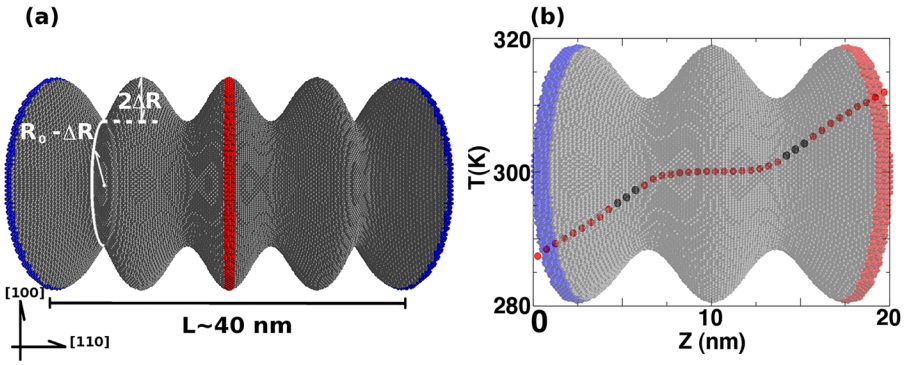


FIG. 1. (a) A CSiNW with amplitude ΔR, mean radius $R_0 = 10$ nm, and inner channel radius $R_0$-ΔR. All wires have a wavelength of 10 nm. (b) Temperature profile for a CSiNW.

wire's length; the mean radius is taken as 10 nm, and the corrugation amplitude is varied from zero to 3.75 nm. All MD calculations are performed using the LAMMPS package[19] using the Stillinger-Weber potential and a time step of 2 fs. The wires were obtained from a perfect crystal and patterned according to Eq. (1), after which they were thermalized using constant temperature and stress MD simulations at T = 300 K and zero external pressure. Thermal transport is studied using a method proposed by Müller-Plathe[20] that generates a heat flux via the periodic exchange of atomic velocities in heat exchange regions. Colored as red and blue in Fig. 1(a), the heat exchange regions correspond to corrugation crests. Throughout the simulation, a Nosé-Hoover thermostat with a weak coupling constant of 10 ps is applied to avoid potential energy drifts.

Velocities are exchanged every 20 fs for the duration of the simulation. Decreasing the swapping period to 4 fs with the corresponding increase in heat flux does not alter our results,[24] indicating that our simulations are within the linear (Fourier) regime between heat flux and temperature gradient. Once the system reaches steady state (within 1 ns), the heat current in the longitudinal direction is computed from the energy exchanged due to velocity swapping per unit time and temperature profiles are computed from atomic velocities. These quantities are averaged for 2 ns after steady state is achieved.

Conventionally, using the heat current and the resultant difference in temperature, the thermal conductance can be calculated by $G_T = \dot{Q}/\nabla T$. In our case, the temperature difference is defined from regions within the troughs of the corrugation, colored in black in the temperature profile in Fig. 1(b). This yields the effective conductance of a single corrugation between the heat exchange regions. We favor conductance instead of conductivity due to the arbitrariness in defining cross-sectional areas in our nanostructured materials.

Black triangles in Fig. 2 show the thermal conductance of the corrugated nanowires as a function of the corrugation amplitude; green and blue squares show values for smooth wires with diameters equal to those of the inner channel ($R_0$-ΔR) and the maximum diameters ($R_0 + \Delta R$) of the corresponding corrugated wires, respectively. Interestingly, the conductance of the corrugated wires falls below the equivalent inner channel values, despite the larger effective cross-sectional area in the corrugated wires. To provide an additional reference for the reduction in conductance, consider a simple model that neglects radial temperature gradients and assumes diffusive behavior. Our wires can then be considered as a set of thermal resistors, with varying cross-sectional areas arranged in series. The overall resistance of such an arrangement is given by

$$\frac{1}{G_T} = \sum_i^n R_i = \rho \sum_i^n L_i/A_i, \tag{2}$$

where the thickness L and thermal resistivity $\rho$ of each element is constant. Thus, predicted conductance is $G_T = [\frac{\rho \times L}{\langle A \rangle}]^{-1}$. From this relation and Eq. (1), we can then define the effective cross-sectional area for thermal transport in the wires from point $z_1$ to $z_2$,

$$\langle A \rangle = \left( \frac{1}{z_2 - z_1} \int_{z_1}^{z_2} \frac{dz}{\pi (R_0 + \Delta R \cos(2\pi z/\lambda))^2} \right)^{-1}. \tag{3}$$

This diffusive model assumes that each section uses its entire cross-section fully for transport and predicts a weak reduction in conductance with increasing corrugation shown as a dashed line in Fig. 2.

Our results show that a corrugation of less then 4 nm can lead to a ~4-fold reduction in conductance from the smooth wire with mean radius ($R_0 = 10$ nm). Contrasting the nanoengineered wires with the smooth inner channel-equivalent ones, the conductance reduction is 30% for the two largest corrugation amplitudes. To understand the microscopic

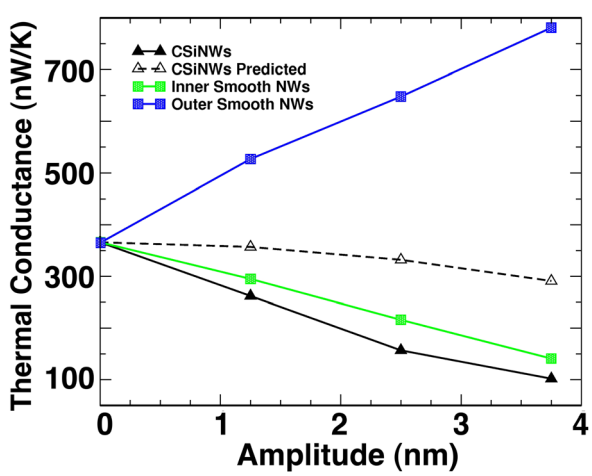


FIG. 2. Thermal conductance values of corrugated Si nanowires (black triangles) lie below the range given by smooth wires with radius $R_0$-ΔR (green squares) and smooth wires with radius $R_0 + \Delta R$, as well as below values predicted from the reduction in effective cross-sectional area (dashed).

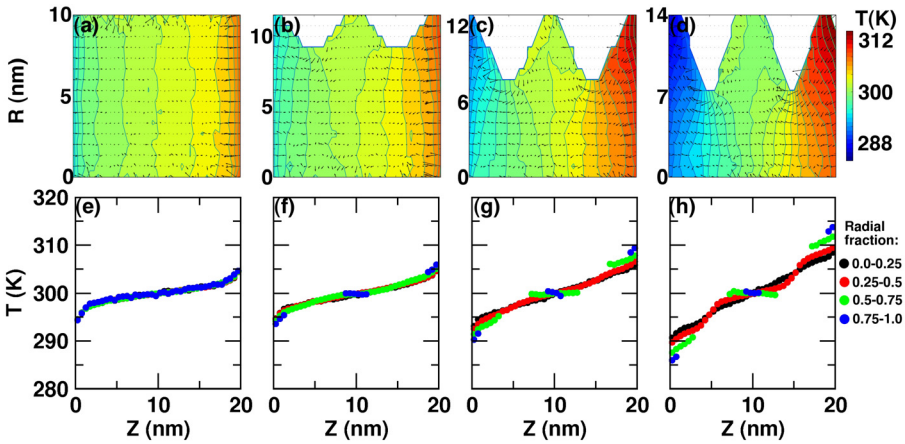


FIG. 3. (a)–(d) Two-dimensional temperature maps within the nanowires. (e)–(h) One-dimensional temperature profiles at different radii illustrate the non-linear and non-monotonic behavior induced by the ridges. The smooth wire (a) is radially homogenous; however, in the corrugated wires, heterogeneity is observed within the ridges in the form of inverted temperature gradients.

origin of the observed reduction in thermal conductance, we analyze spatially resolved local temperature (Fig. 3) and heat current (Fig. 4) within the wires. Due to the cylindrical symmetry of our nanostructures we present values averaged with respect to azimuthal angle, as well as averaged across the plane of symmetry along the transport direction (heat flows from the middle of the simulation cell to both sides). The importance of a full space map is apparent. While cross-section averaged temperature profiles simply show a flattening in the gradients, the spatially resolved profiles unveil the composite nature of this effect.

The local temperature maps show a transition between a spatially uniform temperature gradient (Fig. 3(a)) and heat current (Fig. 4(a)) for smooth wires to increasing heterogeneity and inverted temperature gradients with increasing corrugation. As expected, the temperature gradient along the transport direction and local heat current are larger at the constrictions of the corrugation. Remarkably, for all corrugations we observe temperature gradient inversion within the ridges. This is a manifestation of the ballistic nature of phonon heat transport and a consequence of the fact that ridge size is smaller than the phonon mean free path. Silicon has an effective mean free path of at least 300 nm in the bulk[21] and this value is reduced in nanowires due to surface scattering.[22] This type of behavior could potentially be observable experimentally with techniques such as scanning joule expansion microscopy, which can achieve mK temperature resolutions and a spatial resolution of several nm.[23]

Coupled with significant inverted gradients in the temperature profiles (up to 10% of the total gradient) is the development of an inverted heat current vortex within the crest of the corrugations. We observe a transition of heat current maps conformal to the wire shape at small corrugations to one in which the heat flux separates into a conformal component and vortex at the top of the ridges. This heat "flow detachment" and vorticity is analogous to fluid flow in corrugated pipes in which laminar flow in the central channel makes the transition to turbulent flow inside the corrugations.

Figures 4(e)–4(h) show the overall longitudinal heat current profiles (black lines) and the heat current in a cylindrical region of the inner channel, with radius $R_0$-$\Delta R$ (red lines). We observe that the inner channels carry approximately 80% of the heat even at the ridges where it only represents between 20% and 60% of the total cross-sectional area. Interestingly, the effect of the corrugation on the transport in the inner channel does not depend strongly on corrugation amplitude. This, together with the thermal conductance values, indicates that the reduction in conductance relative to a smooth nanowire saturates as flow detachment and vorticity develop in the ridges. This point of diminishing returns leads

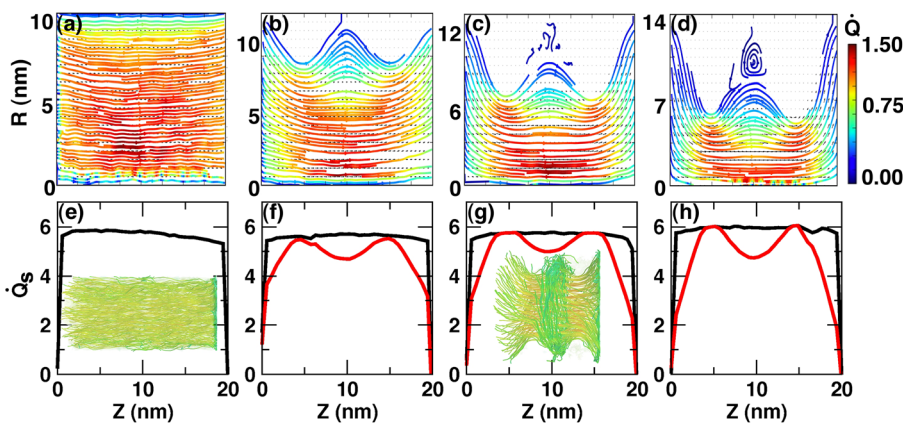


FIG. 4. (a)–(d) Pseudo-atomic heat current streamlines, colored in terms of longitudinal contributions with units of $10^{-19}$ W m. (e)–(h) Longitudinal heat current integrated for various cross-sections ($10^{-16}$ W m). Heat current is primarily concentrated in the inner channel, only extending partially into the ridges. For all corrugation amplitudes, the ridges modulate heat current by approximately 20%. Increasing amplitude does not necessarily improve reduction in thermal transport due to heat current separation within the ridges. Insets in (e) and (g) show the heat current in three dimensions within the respective wires.[24]

to a 30% reduction in thermal conductance for corrugated wires with a cross-sectional area ratio $A_{max}/A_{min}$ greater than about 3.

In summary, by means of non-equilibrium MD simulations we show that nanoengineered corrugations reduce thermal conductance in Si nanowires by a factor of ~4 relative to a wire with the mean radius ($R_0$) and by up to 30% relative to a wire with the minimum radius ($R_0$-$\Delta R$). The only approximations in our simulations are (1) the use of classical (as opposed to quantum) dynamics, which is known to have a negligible effect in thermal transport in Si,[11] and (2) the interatomic potential. As a result, all phonon processes are captured explicitly and without additional approximations. As seen in previous studies,[12,13] increasing corrugation amplitude beyond a saturation limit does not improve the degree of thermal transport reduction. Our atomistic simulations provide a detailed understanding of this fundamental limit. We find this limit to be due to atomic heat current separation within the corrugated ridges that acts as a boundary condition for the heat flow in the inner channel. At larger corrugation amplitudes heat current vortices are observed, similar to behavior in fluid flow through corrugated pipes. These phenomena manifest as inverted gradients in the locally resolved temperature profiles, which could be observed experimentally. This enhanced understanding of heat current behavior in engineered structures with nanoscale modulations can contribute to the development or optimization of devices with applications in energy-conversion and electronics.

This work was supported by the US National Science Foundation, Division of Electrical, Communications and Cyber Systems EECS-1028667 and by US Air Force Office of Scientific Research via Grant No. FA9550-11-0079. Computational resources from nanoHUB.org are gratefully acknowledged.

[1]A. Shakouri, Proc. IEEE **94**(8), 1613–1638 (2006).
[2]D. G. Cahill, W. K. Ford, K. E. Goodson, G. D. Mahan, A. Majumdar, H. J. Maris, R. Merlin, and S. R. Phillpot, J. Appl. Phys. **93**(2), 793 (2003).
[3]D. Li, Y. Wu, P. Kim, L. Shi, P. Yang, and A. Majumdar, Appl. Phys. Lett. **83**(14), 2934 (2003).
[4]Y. Cui and C. M. Lieber, Science **291**, 851–853 (2001).
[5]J. Lim, K. Hippalgaonkar, S. C. Andrews, A. Majumdar, and P. Yang, Nano Lett. **12**(5), 2475–2482 (2012).
[6]L. Liu and X. J. Chen, J. Appl. Phys. **107**(3), 033501 (2010).
[7]M. Kazan, G. Guisbiers, S. Pereira, M. R. Correia, P. Masri, A. Bruyant, S. Volz, and P. Royer, J. Appl. Phys. **107**(8), 083503 (2010).
[8]M. Luisier, J. Appl. Phys. **110**(7), 074510 (2011).
[9]P. Martin, Z. Aksamija, E. Pop, and U. Ravaioli, Phys. Rev. Lett. **102**(12), 125503 (2009).
[10]A. I. Hochbaum, R. Chen, R. D. Delgado, W. Liang, E. C. Garnett, M. Najarian, A. Majumdar, and P. Yang, Nature **451**(7175), 163–167 (2008).
[11]D. Donadio and G. Galli, Phys. Rev. Lett. **102**(19), 195901 (2009).
[12]A. L. Moore, S. K. Saha, R. S. Prasher, and L. Shi, Appl. Phys. Lett. **93**(8), 083112 (2008).
[13]D. L. Nika, A. I. Cocemasov, C. I. Isacova, A. A. Balandin, V. M. Fomin, and O. G. Schmidt, Phys. Rev. B **85**(20), 205439 (2012).
[14]Y. Zhou, B. Anglin, and A. Strachan, J. Chem. Phys. **127**(18), 184702 (2007).
[15]G. Fabbri, Int. J. Heat Mass Transfer **43**(23), 4299–4310 (2000).
[16]S. A. Loh and H. M. Blackburn, Phys. Fluids **23**(11), 111703 (2011).
[17]K. Arora, R. Sureshkumar, and B. Khomami, J. Non-Newtonian Fluid Mech. **108**(1–3), 209–226 (2002).
[18]C. Blanc, A. Rajabpour, S. Volz, T. Fournier, and O. Bourgeois, Appl. Phys. Lett. **103**(4), 043109 (2013).
[19]S. Plimpton, J. Comput. Phys. **117**(1), 1–19 (1995).
[20]F. J. Müller-Plathe, Chem. Phys. **106**(14), 6082 (1997).
[21]Y. S. Ju and K. E. Goodson, Appl. Phys. Lett. **74**(20), 3005 (1999).
[22]K.-H. Lin and A. Strachan, Phys. Rev. B **87**(11), 115302 (2013).
[23]J. Varesi and A. Majumdar, Appl. Phys. Lett. **72**(1), 37–39 (1998).
[24]See supplementary material at http://dx.doi.org/10.1063/1.4844995 for additional simulation and analysis details.